Springer

KSME

Journal of Mechanical Science and Technology 28 (10) (2014) 4083~4090
www.springerlink.com/content/1738-494x
DOI 10.1007/s12206-014-0921-9

Numerical and experimental studies on the mixing characteristics of two jets with inclined angles in a rectangular chamber †

Doo-Hee Han[1], Jun-Su Shin[1], Jeong-Seok Kang[1], Jung-Shin Park[1], Sun-Sang Park[1], Jae-Su Kwak[2], Hong-Gye Sung[2,*] and Ho-Jin Choi[3]

[1]*Department of Aerospace and Mechanical Engineering, Korea Aerospace University, Gyeonggi, 412-791, Korea*
[2]*School of Aerospace and Mechanical Engineering, Korea Aerospace University, Gyeonggi, 412-791, Korea*
[3]*Agency for Defense Development, Daejeon, 305-600, Korea*

(Manuscript Received November 12, 2013; Revised May 26, 2014; Accepted June 20, 2014)

Abstract

Mixing characteristics in a rectangular chamber are investigated using experimental and numerical methods. A mixing chamber with an axial inlet (representing fuel inlet) and a side inlet (representing air inlet) is designed. Two jets with different momentum ratios through the two inlets are mixed in the chamber. Computational fluid dynamic simulation is validated by experimental data of particle image velocimetry that measures flow velocity distribution. The momentum ratios of the two jets and the height of the axial inlet significantly influence the penetration depth of axial jet into the mixing chamber and the pressure drops at recirculation zones.

Keywords: Mixing characteristics; Jet impingements; Inclined jets; Computational fluid dynamics (CFD); Particle image velocimetry (PIV); Recirculation

1. Introduction

A ducted rocket is a ramjet propulsion system that uses intake air and fuel from a metalized solid gas generator [1]. Metal particles are applied to improve specific impulses and enhance combustion stability by particle laden flow [2]. A ducted rocket typically consists of two combustion chambers. The primary chamber is a fuel-rich gas generator that provides fuel-rich, gas-carrying metal particles into the secondary chamber. The secondary chamber, which is the focus of this study, has an air inlet duct and a fuel orifice connected to the primary chamber. In consideration of the long burn time of metal particles compared with that of gas-phase fuel, fuel and oxidizer are mixed properly by using a recirculation zone in a small volume [3]. Consequently, a well-designed secondary chamber plays an important role in for the complete combustion of particles.

Using the experimental approach, Hsieh et al. [4] visualized flow by laser Doppler velocimetry to study the mixing characteristics in the secondary chamber of a ducted rocket. Stowe et al. conducted a water tunnel test [5].

Using the numerical approach, Stowe et al. [6] conducted an ignition test with carbon particles to measure combustion efficiency and compared it with experiments to evaluate its performance. Ristori et al. [7] adopted a numerical method to vary the shape of ducted chambers and check the burning efficiency. Nakayama et al. [8] conducted an ignition test with a glycidyl azide polymer solid propellant and studied mixing characteristics and ignition delay using a numerical method.

In this study, the detailed mixing characteristics of unburned fuel and air in the secondary chamber are analyzed. In this parametric study, the height of the injection orifice, as well as the momentum ratio of fuel and air, is selected as a design parameter. The mixing characteristics are dominantly influenced by the height of the orifice because the size of the recirculation zone varies depending on the location. For reference, an inclined height of a 25% chamber diameter, which has reasonable recirculation zone, is used [9]. For the working fluid of the fuel inlet orifice, air is chosen instead of unburned fuel for experimental convenience. Numerical and experimental methods are applied to investigate the mixing characteristics of fuel and air to velocity ratios and fuel orifice heights in the secondary chamber.

2. Experimental study

In the experimental study, the particle image velocimetry (PIV) technique is applied to investigate the flow-mixing characteristics in the secondary combustor model of a ducted rocket. Fig. 1 presents the schematic of the PIV experimental setup used in this study. Dual-pulse Nd:YAG laser (Ever-Green 145, Quantel) is installed on the upper side of the test

*Corresponding author. Tel.: +82 2 300 0104, Fax.: +82 2 3158 4429
E-mail address: hgsung@kau.ac.kr
† Recommended by Associate Editor Yang Na

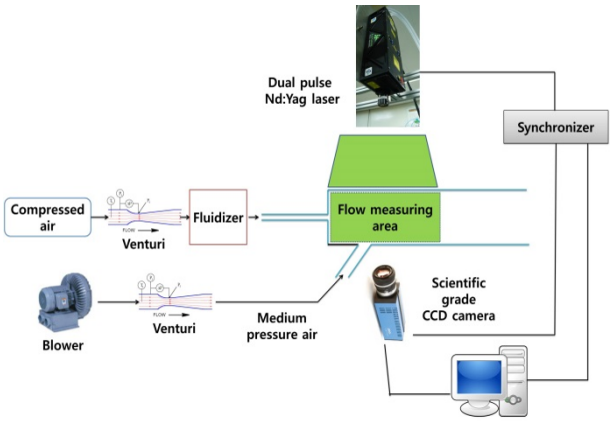

Fig. 1. Schematic of the PIV experimental setup.

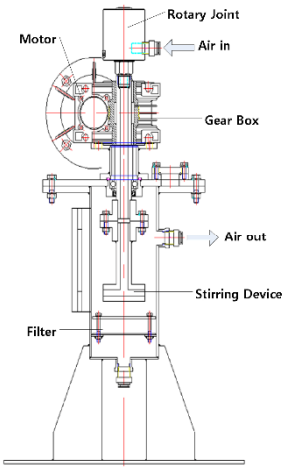

Fig. 2. Schematic of the PIV particle fluidizer.

section and provides a thin-light sheet in the flow measurement area. Spheric polystyrene particles with a diameter of 5 μm are selected as the PIV seeding particle. To float the PIV seeding particle uniformly in the measurement area, an in-house-made fluidizer (Fig. 2) is installed to supply the seeding particle to the axial inlet duct.

A laser pulse and a charge-coupled device (CCD) camera (PCO 1600, PCO.) shutter are synchronized by a pulse delay generator (9514 Pulse Generator, Quantum). Two pictures are taken by the CCD camera with a short time interval (6 μs). The displacements of particles in the two pictures are analyzed by a PIV data reduction program (INSIGHT 4G, TSI) to calculate the flow vector field.

Fig. 3 shows the test parameters in this study. The air velocities of the axial and side inlets are defined as V_1 and V_2, respectively. The cross-section of the mixing chamber is square, and the height (H) and depth are 60 mm. The measurement plane is located at the center of the duct, as shown in Fig. 3. The location of the axial inlet (h = 25% and 50% of H), the angle of the side inlet (θ = 60 degrees), and the location of the side inlet (L = 60% of H) are defined in Fig. 3. The side inlet flow is supplied by a blower, and the velocity of the side inlet flow in the flow mixing zone is fixed at 30 m/s. The air

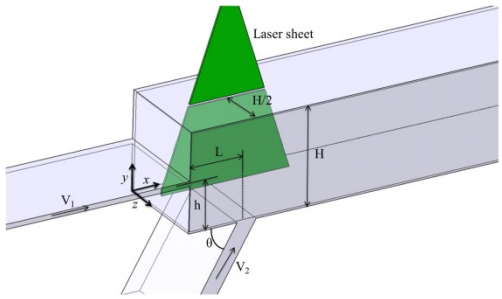

Fig. 3. Laser sheet in the experimental setup.

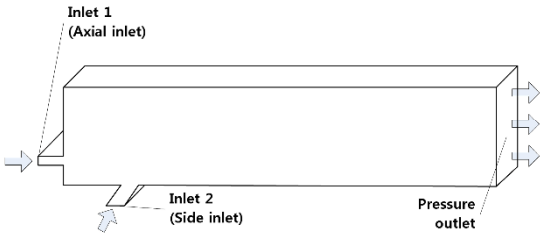

Fig. 4. Schematic of the secondary chamber.

velocity of the axial inlet duct varies from 45 m/s to 150 m/s and results in velocity ratios (V_1/V_2) of 1.5, 3.0, and 5.0.

3. Numerical study

Mixing phenomena should be analyzed in detail if calculation is conducted minutely. In the simulation, a commercial computational fluid dynamic (CFD) code ANSYS FLUENT 12.1 is implemented. A k-epsilon turbulence model with enhanced wall functions is adopted to analyze the mixing characteristics. This model is a relatively recent development compared with the standard k-epsilon, which is a semi-empirical approximation based on solving transport equations for the turbulence kinetic energy, k, and dissipation rate, epsilon, with empirical constants. Compared with the standard model, the current model has an improved equation for epsilon and variable turbulence viscosity, which is constant in the standard model. Therefore, the current model has better performance for flows that involve large rotation and recirculation. A detailed description can be found in Ref. [11]. To obtain accurate calculations, third-order monotonic upstream-centered schemes for conservation laws are applied for spatial discretization [12]. Specific heat and viscosity are calculated by piecewise-polynomial and Sutherland's law, respectively [13].

Fig. 4 shows the 3D computational domain used to simulate the flow mixing inside the secondary chamber. The domain has approximately 3.1 million structured cells and contains a high-resolution grid near the axial inlet (inlet 1) and side inlet (inlet 2), where rapid flow mixing occurs, to reduce computational-scale efforts. The boundary condition uses measured parameters in the experimental study for precise simulation. The mass flow rate condition is applied for inlets, which are

Table 1. Boundary conditions used in each case.

Case	Inlet 1 position, vel. ratio (Momentum ratio)	Mass flow rate of inlet 1 (kg/s)	Mass flow rate of inlet 2 (kg/s)
Case 1	25%, 1:5.0 (1:8.5)	0.034607	0.020520
Case 2	25%, 1:3.0 (1:2.8)	0.014458	0.015782
Case 3	25%, 1:1.5 (1:0.8)	0.007179	0.013888
Case 4	50%, 1:50 (1:8.5)	0.0341960	0.019911
Case 5	50%, 1:3.0 (1:2.8)	0.017748	0.018719
Case 6	50%, 1:1.5 (1:0.8)	0.009089	0.016753

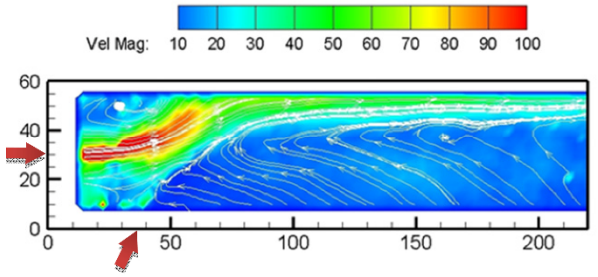

(a) 50% height, velocity ratio = 1:5

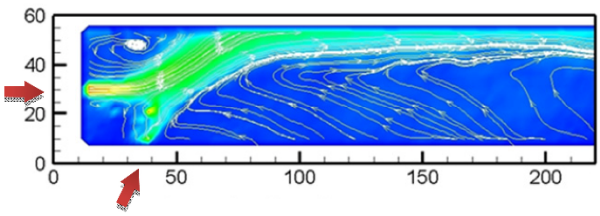

(b) 50% height, velocity ratio = 1:3

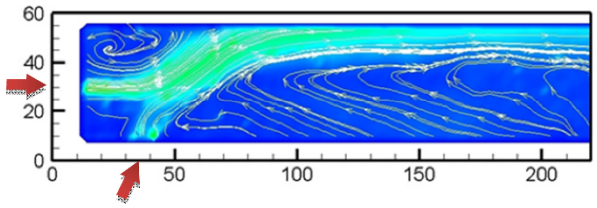

(c) 50% height, velocity ratio = 1:1.5

Fig. 5. Velocity contour measured by PIV at 50% height.

measured by a Venturi meter for every experiment. The outlet has a pressure condition and is fixed to atmospheric pressure because experiments are set to blast gas into the open area. The detailed parameters of the boundary conditions used in this study are summarized in Table 1.

4. Comparison between numerical results and experimental measurements

Fig. 5 presents the experimentally measured velocity data, and Fig. 6 shows the numerically calculated velocity distribution at the center of the Z-plane with a 50% height of inlet 1. These results are comparable with an almost similar flow

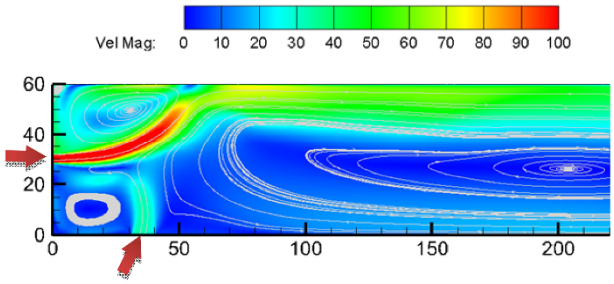

(a) 50% height, velocity ratio = 1:5

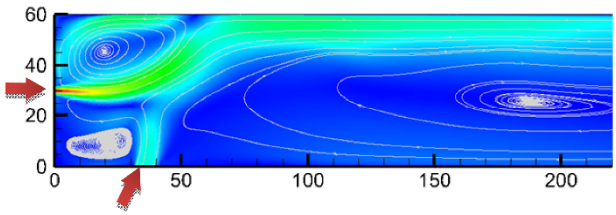

(b) 50% height, velocity ratio = 1:3

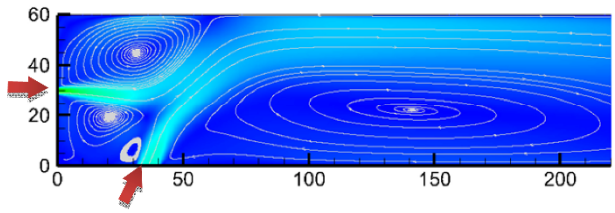

(c) 50% height, velocity ratio = 1:1.5

Fig. 6. CFD results of the velocity contour at 50% height.

structure, given that the experiment cannot acquire particle data near the wall. Experimental data have weak or no recirculation zone on the upper side, whereas numerical results have a strong zone. However, numerical and experimental results have the same tendency. When a high speed jet from inlet 1 crashes with a relatively low speed of air from inlet 2, it rises and attaches to the upper wall. Figs. 7 and 8 present a velocity contour in case of a 25% height. However, the velocity contour is slightly different at a velocity ratio of 1:5. The core of the main structure rises fast in case of simulation. Experimental results with 1:5 velocity ratios have wide flow range. Therefore, PIV method detects the velocity of a particle with its own inertia moments depending on the poly (methyl methacrylate) particle size. As a result, small particles follow the gas phase exactly, whereas large particles ignore the flow direction changes and penetrate the inertia momentum. The experimental and numerical results in case of a 1:5 velocity ratios with 25% height support this finding. Although the core of the main flow structure is slightly different, the numerical results are marginally acceptable than the experimental results. A large velocity ratio causes a steep rise of the main flow jets and early attachment at 50% height. This case has a completely adverse tendency compared with that at 25% height. Therefore, high-momentum jets penetrate deeply. A detailed discussion on the reason for this phenomenon will be given in

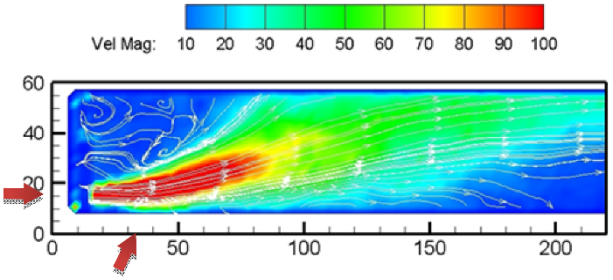

(a) 25% height, velocity ratio = 1:5

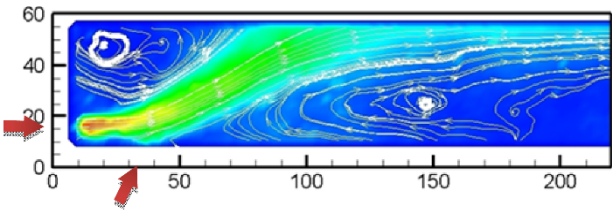

(b) 25% height, velocity ratio = 1:3

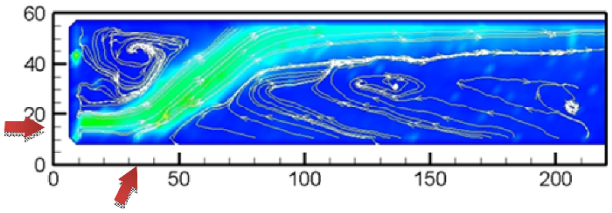

(c) 25% height, velocity ratio = 1:1.5

Fig. 7. Velocity contour measured by PIV at 25% height.

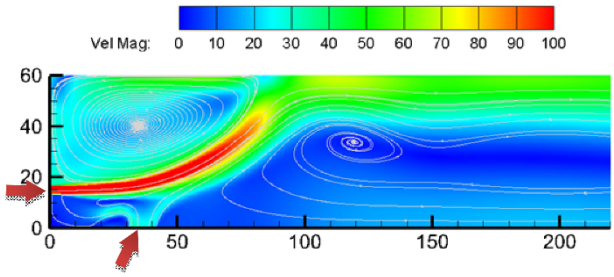

(a) 25% height, velocity ratio = 1:5

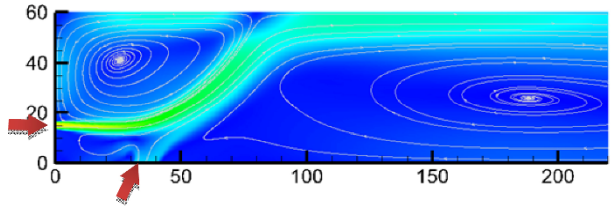

(b) 25% height, velocity ratio = 1:3

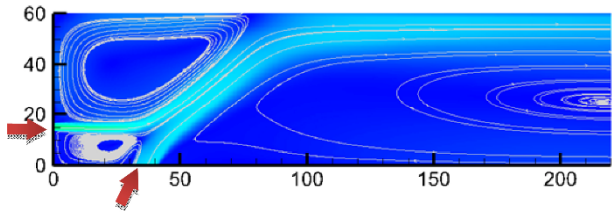

(c) 25% height, velocity ratio = 1:1.5

Fig. 8. CFD results of the velocity contour at 25% height.

the next chapter.

Figs. 9 and 10 present the velocity distribution along the center line of inlet 1 to quantitatively compare the penetration depths of jets quantitatively. Distance is normalized with height H. Fig. 9 presents the velocity distribution at 50% height of inlet 1. When the velocity ratio is 1:5, case (a) shows a similar velocity order, except at approximately 40 mm. Data are lacking between 0 mm and 15 mm at the experimental curve because the particle velocity near the wall cannot be is unable to measured. The penetration depth in the experiments is deeper than that in the simulation. Case (b), with a velocity ratio of 1:3, is almost comparable to with case (a). The experimental results show a high velocity at approximately 40 mm distance. Case (c) denotes a different trend. A gap exists between 0 mm and 50 mm. The simulation predicts faster momentum diffusion as the velocity curve drops rapidly than that in the experiment. However, the simulation shows a similar penetration depth to that of the experimental data at approximately 80 mm.

For the 25% height of inlet 1, penetration agrees well with the velocity ratios of 1:3 and 1:1.5, as shown in Fig. 10. However, some differences are observed in case Fig. 10(a) with a velocity ratio of 1:5. The experiment measures the particle velocity and not the direct velocity of the gas phase. A detailed analysis will be discussed in the next chapter.

5. Mixing characteristics

5.1 Effect of velocity ratios on axial and side inlets

Flow velocity profiles at the centerline are extracted from the computational domain and PIV data to examine the penetration depth, which is defined by the end point of decreasing velocity that is less than 5% of the speed of inlet 1. Figs. 11 and 12 show the experimental and numerical penetration depths at inlet heights of 50% and 25%, respectively. In Fig. 11, the depth decreases from 86 mm to 48 mm as the velocity ratio increases from 1:1.5 to 1:5. This case may be considered an opposite trend on the basis of the velocity ratio because a large momentum of the main flow shows more penetration depth. However, a high velocity induces a strong recirculation and decreases the pressure in the recirculation zone to pull the main flow to float to the zone. As a result, a high velocity ratio has a short penetration depth at 50% height of inlet 1.

Fig. 12 presents a contrast tendency that has an increasing depth from 59 mm to 62 mm with an increasing velocity ratio from 1:1.5 to 1:5. This tendency can be explained by the pressure drop rate near the jet. Fig. 13 shows the minimum pressure in the upper recirculation zone according to velocity ratios.

The pressure drops in the case of 50% height are larger than those in the case at 25% height, which results in different ten-

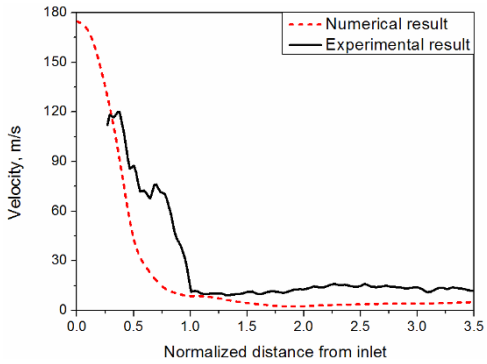

(a) 50% height, Velocity ratio = 1:5

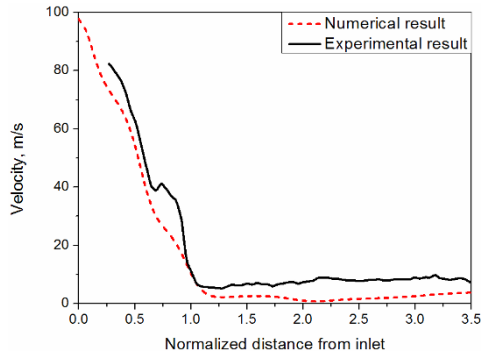

(b) 50% height, Velocity ratio = 1:3

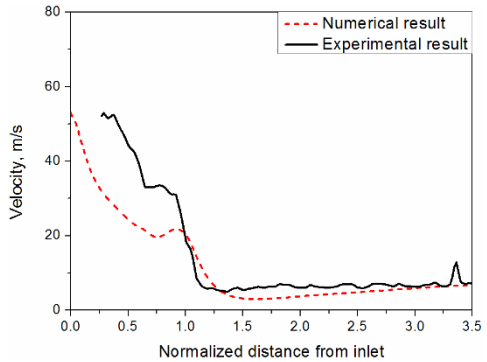

(c) 50% height, Velocity ratio = 1:1.5

Fig. 9. Velocity distribution at the centerline of inlet 1 at 50% height.

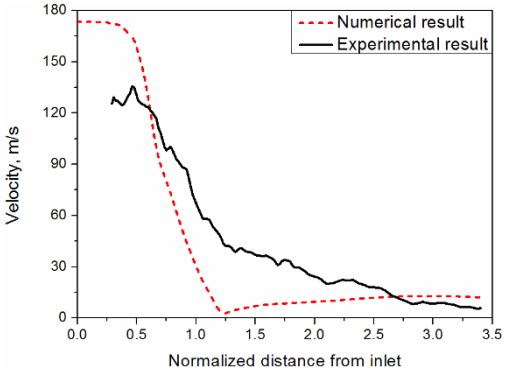

(a) 25% height, Velocity ratio = 1:5

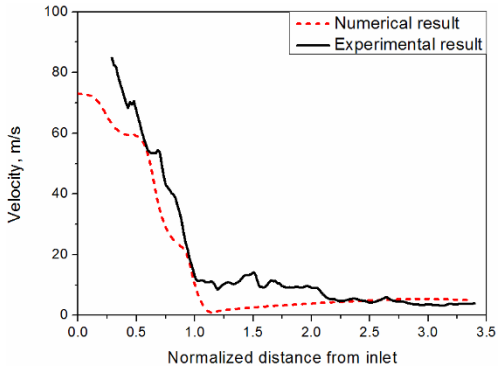

(b) 25% height, Velocity ratio = 1:3

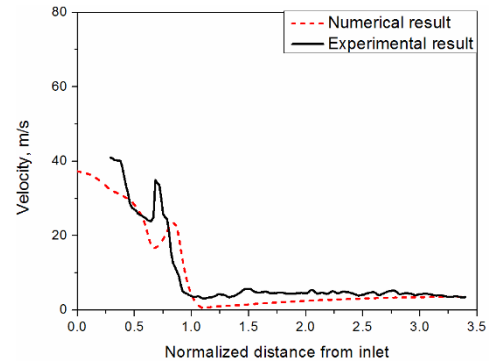

(c) 25% height, Velocity ratio = 1:1.5

Fig. 10. Velocity distribution at the centerline of inlet 1 at 25% height.

dencies. The 25% height has more influence on the flow momentum than pressure drop, which has an opposite tendency at 50% height.

5.2 Effect of recirculation intensity

Recirculation at the fore dome (upper-left side in a contour) of the secondary chamber plays an important role to establish high-combustion efficiency in the secondary chamber because it extends the residence time of the combusting particle. Recirculation also affects the curvature of the main stream. Fig. 14 presents the comparison of pressure distribution between two different heights of inlet 1, that is, 50% and 25%. Pressure in the upper zone of inlet 1 at 50% height decreases to 98000 kPa because of strong recirculation, as presented in Fig.

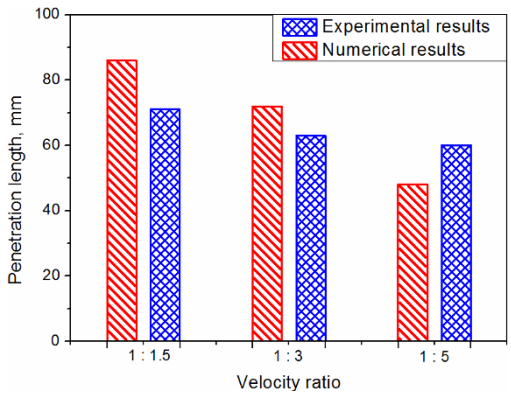

Fig. 11. Penetration depth for 50% height.

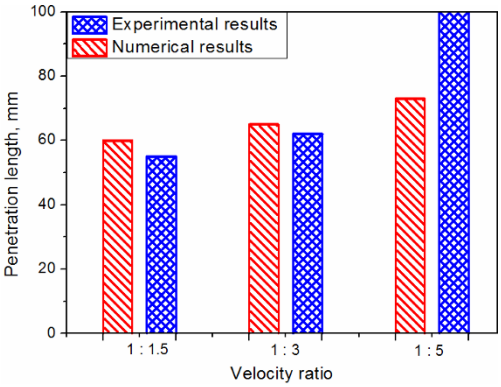

Fig. 12. Penetration depth for 25% height.

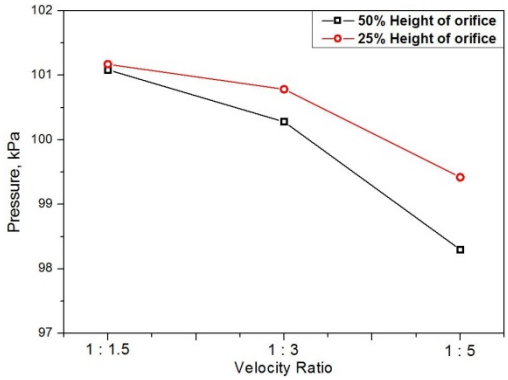

Fig. 13. Pressure drop in the upper recirculation zone.

15. The decrease in pressure in case Fig. 15(b), which has 25% height, is minimal. The reason for this may be that the volume of the upper recirculation zone at 25% height is larger than that at 50% height. Therefore, the recirculating intensity decreases. Fig. 15 shows a Z-direction vorticity to visualize the recirculation intensity. In the upper zone, strong counter-clockwise recirculation is observed because of the shear layer of high-speed flow from inlet 1, whereas weak intensity is detected in the lower zone. The recirculation direction is determined in an opposite direction of the shear flow. As the pressure decreases more in the upper recirculation zone, the main flows are forced backward to the flow direction and attached to the upper wall further upstream than those at the 25% height case. The injection angles from inlet 2 are also affected by pressure drop. The angles are approximately 90°, 70°, and 60° with velocity ratios of 1:5, 1:3, and 1:1.5 respectively. As the angle of inlet 2 is 60°, the flow leans backward when pressure drops at the fore dome.

5.3 Mixing efficiency

Mixing efficiency is compared at the fore dome. Two air species from inlets 1 and 2 are calculated individually with species transport to visualize the mixing rate. In this study, the normalized mixing efficiency, ζ, is defined as follows:

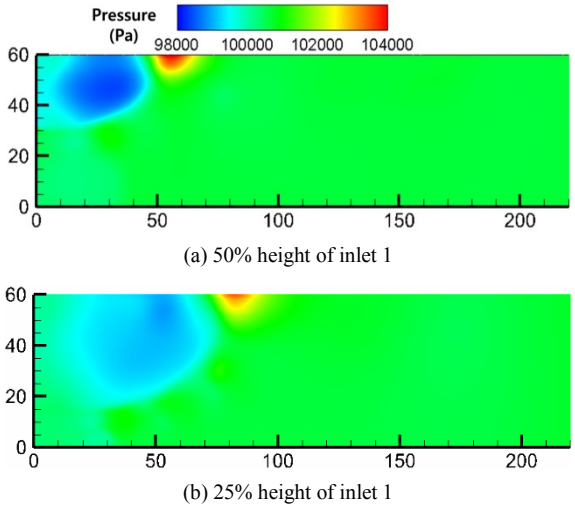

(a) 50% height of inlet 1

(b) 25% height of inlet 1

Fig. 14. Pressure contours at a velocity ratio of 1:5.

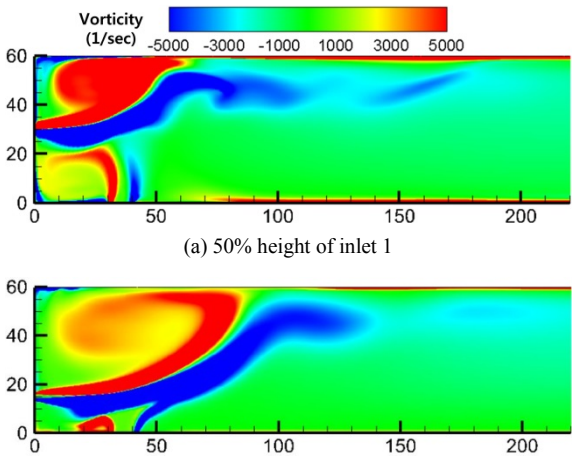

(a) 50% height of inlet 1

(b) 25% height of inlet 1

Fig. 15. Z-vorticity contours at the axial and cross-sections at a velocity ratio of 1:5.

$$\zeta = \frac{MF_2}{\dot{m}_{inlet2} / (\dot{m}_{inlet1} + \dot{m}_{inlet2})},$$

where MF_2 is the mass fraction of air from inlet 2 at the fore dome, and $\dot{m}_{inlet1}$ and $\dot{m}_{inlet2}$ are the mass flow rates of air from inlets 1 and 2, respectively.

Fig. 16 presents the normalized mixing efficiency at the fore dome for all six cases. The 25% height case shows the highest efficiency at 0.555 at a low velocity ratio, but it has the lowest efficiency at a high velocity ratio. The overall tendency shows gradually increasing mixing efficiency for the reference cases (cases 1 to 3), whereas the others (cases 4 to 6) show rapidly decreasing efficiency. The reason for this phenomenon is the different influences from the recirculation zone depending on the height of inlet 1. As mentioned earlier, the 50% height case has strong vorticity with a high velocity ratio at the fore

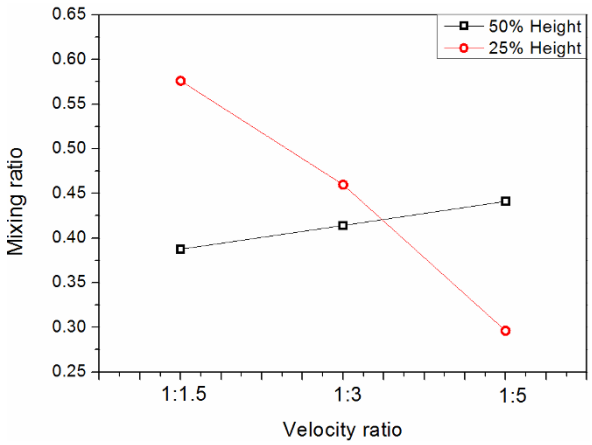

Fig. 16. Normalized mixing efficiency ratio at the fore dome.

dome that causes a short penetration depth with a high velocity ratio. Therefore, a high velocity ratio has strong vorticity, which creates good mixing efficiency. However, the 25% height has an opposite tendency in terms of velocity ratio and vorticity coupling. In the 25% height case, a high velocity only makes flow penetrate deeply, but the mixing efficiency decreases. The influence of velocity ratio on vorticity is also stronger at 50% height than at 25% height based on the comparison of their slopes.

6. Conclusion

The mixing characteristics in the secondary chamber of a ducted rocket are experimentally and numerically studied. The PIV experimental results and CFD results are in a good agreement. The penetration depth of the axial inlet flow, i.e., inlet 1, presents a contrast tendency to velocity ratio at different heights of the axial inlet. The depth of the main stream in case of the 25% height of inlet 1 increases from 59 mm to 62 mm, which is proportional to the velocity ratio. However, the depth decreases from 86 mm to 48 mm in case of the 50% height. A larger pressure drop occurs in the recirculation zone of the 50% height of inlet 1 than in other cases. This phenomenon is supported by the experimental and numerical results. The normalized mixing efficiency depends on the velocity ratio of the axial and side inlets. The mixing characteristics studied in this work can be applied when designing high-velocity mixing chambers.

References

[1] M. Nagai, Y. Muroi, Y. Suti, W. Saito, M, Tanabe and T kuwahara, Ignition and combustion characteristic in the recirculation zone of ducted rockets –effects of titanium, Magnesium and Boron Particles Addition-, *45th AIAA/ASME/SAE/ASEE Joint Propulsion Conference & Exibit*, Denver, Colorado (2009) AIAA 2009-5388.

[2] T. Feraille, G. Casalis and J. Dupays, Particle effects on solid-propellant motors flow stability, *38th AIAA/ASME/SAE/ASEE Joint Propulsion Conference & Exibit*, Indianapolis, Indiana (2002) AIAA 2002-3611.

[3] T kuwahara, K. Obuchi and M. Tanabe, Mass transfer in the recirculation zone of ducted rocket, *44th AIAA/ASME/SAE/ASEE Joint Propulsion Conference & Exibit*, Hartford, CT (2008) AIAA 2008-4892.

[4] W. H. Hsieh, C. L. Chuang, A. S. Yang, D. L. Cherng, V. Yang and K. K. Kuo, Measurement of flowfield in a simulated solid-propellant ducted rocket combustor using laser doppler velocimetry, *AIAA/ASME/SAE/ASEE 25th Joint Propulsion Conference*, Monterey, CA (1989) AIAA-89-2789.

[5] R. A. Stowe, A. DeChamplain, A. E. H. J. Mayer and S. F. Niemeijer, *Modelling and Flow Visualization in a Ducted Rocket Combustor*, AIAA-98-3768.

[6] R. A. Stowe, C. Dubois, P. G. Harris, A. E. H. J. Mayer, A. de Champlain and S. Ringuette, Performance prediction of a ducted prediction of a ducted rocket combustor using a simulated solid fuel, *Journal of Propulsion and Power*, 20 (5) (2004) 936-944.

[7] A. Ristori and E. Dufour, Numerical simulation of ducted rocket motor, *37th AIAA/ASME/SAE/ASEE Joint Propulsion Conference & Exhibit*, Salt Lake City, Utah (2011).

[8] H. Nakayama, Y. Ikegami, A. Yoshida, K. Koori, K. Watanabe, H. Tokunaga, H. Shimizu and S. Kanaizumi, Full-scale firing tests of variable flow ducted rocket engines employing GAP solid fuel gas generator, *45th AIAA/ASME/SAE/ASEE Joint Propulsion Conference & Exhibit*, Denver, Colorado (2009).

[9] Z. Xia, J. Hu, D. Fang, J. Guo and W. Zhang, Combustion study of the boron particle in the secondary chamber of ducted rocket, *42nd AIAA/ASME/SAE /ASEE Joint Propulsion Conference & Exhibit*, Sacramento, Califonia, AIAA 2006-4445.

[10] *ANSYS FLUENT 12.0 Theory Guide*, April (2009).

[11] B. Van Leer, Toward the ultimate conservative difference scheme. IV. A Second Order Sequel to Godunov's Method, *Journal of Computational Physics*, 32 (1979) 101-136.

[12] K. Kadoya, N. Matsunaga and A. Nagashima, Viscosity and thermal conductivity of dry air in the gaseous phase, *J. Phys. Chem. Ref. Data,* 14 (4) (1985).

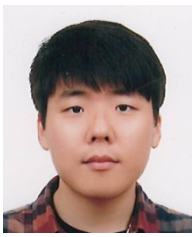

Doo-Hee Han received his B.S. degree from the Department of Aerospace and Mechanical Engineering at the Korea Aerospace University in 2013. He is currently a master candidate in the School of Aerospace and Mechanical Engineering at the Korea Aerospace University in Goyang City, Korea. His research interests are metal particle combustion and numerical simulation.

Jun-Su Shin received his B.S. and M.S. degrees from the Department of Aerospace and Mechanical Engineering at the Korea Aerospace University in 2010 and 2012, respectively. He is currently a Ph.D. candidate in the School of Aerospace and Mechanical Engineering at the Korea Aerospace University in Goyang City, Korea. His research interests include Ram, Scramjet propulsion, DDES simulation, and HEM.

Jeong-Seok Kang received his B.S. degree from in the School of Aerospace and Mechanical Engineering at the Korea Aerospace University in Goyang City, Korea. His research interests are metal particle combustion and numerical simulation.

Jung-Shin Park received his B.S. and M.S. degrees from the Department of Aerospace and Mechanical Engineering at the Korea Aerospace University in 2010 and 2012, respectively. He is currently a Ph.D. candidate in the School of Aerospace and Mechanical Engineering at the Korea Aerospace University in Goyang City, Korea. His research interests are aerodynamics and heat transfer in a gas turbine blade.

Soon-Sang Park received his B.S. degree from the Department of Aerospace and Mechanical Engineering at the Korea Aerospace University in 2013. He is currently a master's candidate in the School of Aerospace and Mechanical Engineering at the Korea Aerospace University in Goyang City, Korea. His research interests are film cooling and heat transfer in a gas turbine blade.

Jae-Su Kwak received his B.S. and M.S. degrees in Mechanical Engineering from Korea University in 1996 and 1998, respectively. He then received his Ph.D. from Texas A&M University in 2002. Dr. Kwak is currently an Associate Professor in the School of Aerospace and Mechanical Engineering at the Korea Aerospace University in Goyang City, Korea. His main research interests include gas turbine heat transfer, heat transfer in a propulsion system, and enhancement of heat transfer.

Hong-Gye Sung received his B.S. degree from the Department of Aerospace Engineering at Inha University in 1984 and his Ph.D. degree in Nuclear and Mechanical Engineering from The Pennsylvania State University in 1999. Dr. Sung worked at the Agency for Defense Development for 22 years (1984–2006) and obtained various research experiences in the fields of high-speed propulsion and rocket propulsion. He is currently a professor in the School of Aerospace and Mechanical Engineering at the Korea Aerospace University in Goyang City, Korea. Dr. Sung's research interests are propulsion, combustion, and its control.

Ho-Jin Choi received his B.S. and Ph.D. degrees in Mechanical Engineering from the Seoul National University in 1998 and 2010, respectively. Dr. Choi is a senior researcher at the Advanced Propulsion Center of the Agency for Defense Development in Daejeon, Korea. He has been working in the field of air-breathing engine, such as Turbo jet, Ramjet, and Scramjet, since 2002. His research interests include combustion and laser diagnostics.